ISSN 0023-1584, Kinetics and Catalysis, 2007, Vol. 48, No. 4, pp. 541–549. © MAIK "Nauka/Interperiodica" (Russia), 2007.
Original Russian Text © A.V. Myshlyavtsev, M.D. Myshlyavtseva, 2007, published in Kinetika i Kataliz, 2007, Vol. 48, No. 4, pp. 576–585.

MECHANISMS OF CATALYTIC REACTIONS

Lateral Interactions in the Adsorption Layer and Critical Phenomena in the Langmuir–Hinshelwood Reaction

A. V. Myshlyavtsev[a,b] and M. D. Myshlyavtseva[a]

[a] *Omsk State Technical University, Omsk, 644050 Russia*

[b] *Institute of Hydrocarbon Processing, Siberian Branch, Russian Academy of Sciences, Omsk, 644040 Russia*

e-mail: myshl@omgtu.ru

Received July 8, 2006

Abstract—The report deals with the effect of the lateral interactions between adsorbed species on the steady state multiplicity area and on the possible rate self-oscillations for a reaction proceeding via the Langmuir–Hinshelwood mechanism. The adsorption layer is modeled as a lattice gas on a square lattice. For irreversible adsorption, the maximum possible number of interior steady states is at least ten. Reaction rate self-oscillations resulting from Andronov–Hopf bifurcation take place for some lateral interaction energy sets. These self-oscillations are associated with a checkerboard-type ordered dense phase existing owing to the attraction between different adsorbed species.

DOI: 10.1134/S0023158407040106

Critical phenomena (steady-state multiplicity, reaction rate self-oscillation, dynamic chaos, etc.) in heterogeneous catalytic systems have been attracting researchers' attention since their discovery in the early 1970s [1–3]. The simplest example is a reaction that is described by the overall stoichiometric equation

$$A_2 + 2B \longrightarrow 2AB \qquad \text{(I)}$$

and proceeds via the standard Langmuir–Hinshelwood (LH) mechanism [1]:

$$\begin{aligned} &(1)\quad A_2 + 2Z \longleftrightarrow 2AZ,\\ &(2)\quad B + Z \longleftrightarrow BZ,\\ &(3)\quad AZ + BZ \longrightarrow 2Z + AB. \end{aligned} \qquad \text{(II)}$$

Here, AZ and BZ are compounds on the surface of the catalyst Z and A_2, B, and AB are compounds in the gas phase. This mechanism describes, in the first approximation, CO oxidation on the surface of platinum-group metals (Pt and Pd).

The LH mechanism implies steady-state multiplicity even for an ideal adsorption layer in the mean-field approximation. This means that there is a region of parameters where the LH reaction mechanism has two steady states. Simple and important to practice, this mechanism has been actively investigated theoretically since the late 1970s to the present day [1–3].

There have been several lines of the theoretical kinetic investigation of heterogeneous catalytic systems. The first line is increasing the number of elementary steps (that is, modifying mechanism (II)) without changing the rate law, written in the form of the law of mass action (LMA), and taking into account the nonisothermicity of the process and the macroinhomoheity in the distribution of the reactants and the catalyst [4–9]. The second line is complicating the adsorption layer model and, accordingly, modifying the rate law. Deviations from the LMA can be due to the limited mobility of adsorbed species, lateral interactions in the adsorption layer, or adsorption-induced surface reconstruction or relaxation. The limited mobility of adsorbed species was taken into account for the first time in a classical work by Ziff et al. [10]. The model presented in that work, named the ZGB model, indicates so-called kinetic phase transitions. This model and its modifications are still being investigated by various methods [11–16]. In recent years, much attention has been focused on the response of various models of reactions proceeding via the LH or a similar mechanism to periodic external actions [15, 17, 18] and to internal noise [19–22].

The effect of lateral interactions on kinetics has also been studied for a long time, since the late 1970s. However, these interactions in deterministic models are usually taken into account by introducing an ad hoc relationship between the activation energies of reaction steps and the reactant coverage of the surface [1, 2, 23]. This approach is quite acceptable and justifiable when there is no detailed information about the microscopic processes on the catalyst surface. However, it would be more correct to take an approach based directly on a microscopic model from which the observed empirical relationships follow without any fitting. Again, this approach is not quite satisfactory. Usually, the lateral interactions in an adsorption layer model are directly taken into account in imitation simulation, in particular, in the construction of imitation models taking into account surface reconstruction [3, 19, 20, 24–27]. At

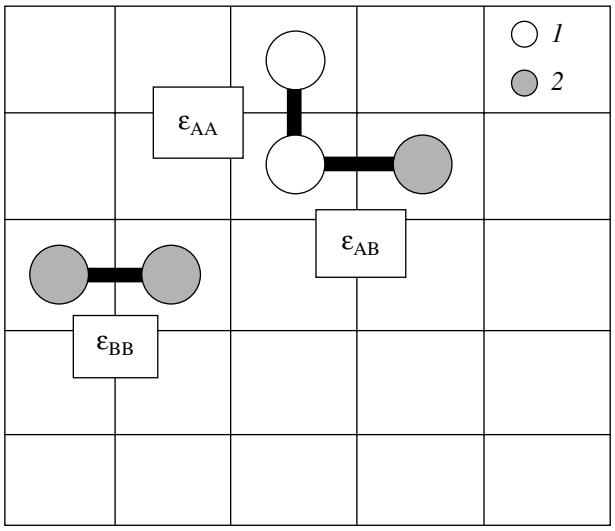

Fig. 1. Lateral interaction types taken into account in the model: (*1*) species A and (*2*) species B.

the same time, there has been no systematic analysis of the effect of lateral interactions in the adsorption layer on the steady-state multiplicity or on the possibility of self-oscillations in the LH reaction.

For an ideal adsorption layer (thermodynamically equilibrated layer such that there are no lateral interactions or surface reconstruction), the kinetic model in terms of the LMA for the LH mechanism can be written as follows [1, 28, 29]:

$$\begin{cases} d\theta_A/dt = 2k_1 P_{A_2}(1-\theta_A-\theta_B)^2 - 2k_{-1}\theta_A^2 - k_3\theta_A\theta_B \\ d\theta_B/dt = k_2 P_B(1-\theta_A-\theta_B) - k_{-2}\theta_B - k_3\theta_A\theta_B, \end{cases} \quad (1)$$

where θ_A and θ_B are the AZ and BZ coverages of the surface, k_1 and k_2 are the adsorption rate constants for the gas-phase compounds A_2 and B, k_{-1} and k_{-2} are the desorption rate constants, k_3 is the rate constant of the third step in mechanism (II), t is time, and P_{A_2} and P_B are the partial pressures of the gas-phase compounds A_2 and B.

The solutions of the set of differential equations (1) are defined in the triangle (reaction simplex) $G = \{(\theta_A, \theta_B) | \theta_A \geq 0, \theta_B \geq 0, \theta_A + \theta_B \leq 1\}$. The simplex G is a positively invariant set for the dynamic set of equations (1); that is, if $\theta_A(0), \theta_B(0) \in G$, then $\forall t > 0$: $\theta_A(t), \theta_B(t) \in G$. This ensures the existence of at least one steady state for the set of equations (1).

For the particular case of $k_{-1} = k_{-2} = 0$, implying that the adsorption of both compounds from the gas phase is irreversible, the set of equations (1) always has two steady-state solutions in both ideal and nonideal cases. Both solutions belong to a simplex boundary: $\theta_{A,1} = 0$, $\theta_{B,1} = 1$; $\theta_{A,2} = 1$, $\theta_{B,2} = 0$. The first steady state is stable, and the second is unstable [1, 29]. At certain parameter values, two interior steady states can exist along with the boundary steady states even for an ideal adsorption layer. For irreversible adsorption, the bifurcation set in the (P_{A_2}, P_B) can be determined in explicit form [1, 29]:

$$P_B = (2k_1 P_{A_2}/k_2)/(1 + (8k_1 P_{A_2}/k_3)^{1/2}). \quad (2)$$

Under the assumption that the adsorption layer is ideal, mechanism (II) cannot describe self-oscillations, as more complicated mechanisms are required [1, 2, 29]. A radically different situation can take place in the case of a nonideal adsorption layer.

Here, we report the effect of the lateral interactions between adsorbed species on the steady-state multiplicity region and on the possible self-oscillations of the rate of a reaction proceeding via the LH mechanism. In our analysis, we used mean-field kinetic equations that account for the lateral interactions through the concentration dependences of rate constants. These constants were calculated directly from a microscopic model of the adsorption layer within transition state theory.

MODEL AND METHOD

The adsorption layer will be modeled as a lattice gas (LG) on a homogeneous square lattice accommodating two types of species. Only the lateral interaction between the nearest neighbors will be considered. The Hamiltonian of this model can be written as

$$H_{eff} = \varepsilon_{AA}\sum_{\langle nn\rangle} n_{A,i}n_{A,j} + \varepsilon_{AB}\sum_{\langle nn\rangle} n_{A,i}n_{B,j} + \varepsilon_{BB}\sum_{\langle nn\rangle} n_{B,i}n_{B,j} - \mu_A\sum_i n_{A,i} - \mu_B\sum_i n_{B,i}, \quad (3)$$

where ε_{AA}, ε_{AB}, and ε_{BB} are the energies of the lateral nearest neighbor interactions (schematized in Fig. 1); $n_{A,i}$ and $n_{B,i}$ are the occupancies of the ith cell (occupancy is equal to unity if the cell is occupied by the species indicated in the subscript; otherwise, it is equal to zero); μ_A and μ_B are the chemical potentials of the adsorbed species A and B; and $\langle nn\rangle$ means summation over all pairs of nearest neighbors on the square lattice. In the last two terms of Hamiltonian (3), summation is performed over all lattice cells. Note that the LG model, which is described by Hamiltonian (3), is equivalent to the spin model with a classical spin S taking values of ±1 and 0, which is known as the Blume–Capel model. In the general case, the Blume–Capel model has a rich phase diagram with several triple critical points.

Obviously, the kinetics of a reacting system described by mechanism (II) depends strongly on the structure of the phase diagram of the adsorption layer. We considered 27 adsorption layer models, in which each of the energies ε_{AA}, ε_{AB}, and ε_{BB} was given a value of 10, –10, or 0 kJ/mol. These values of the lateral interaction energy were chosen for reasons of convenience in demonstrating the potential inherent in the LH mech-

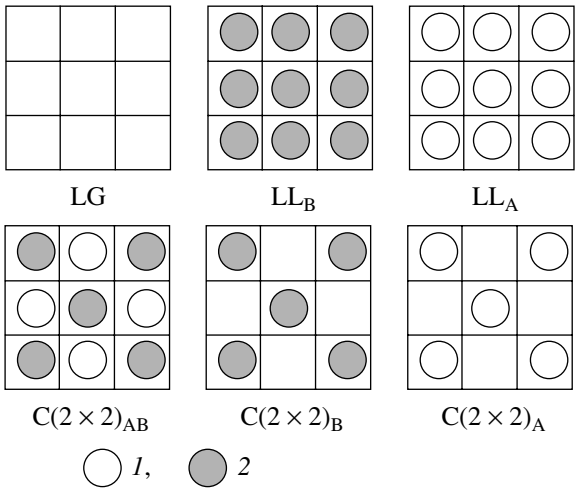

Fig. 2. Structures of phases possible in the model: (*1*) species A and (*2*) species B.

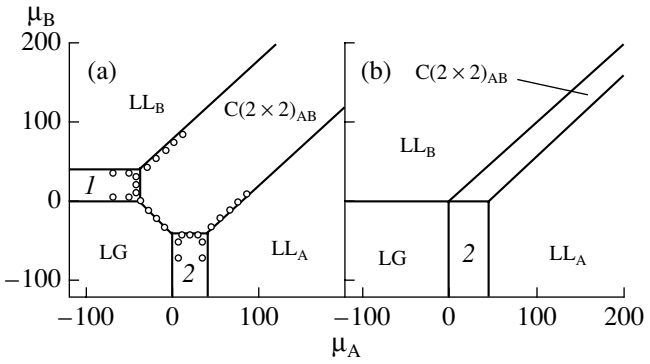

Fig. 3. Phase diagrams on the (μ_A, μ_B) plane for the lateral interaction energy sets (a) (10, –10, 10) and (b) (10, 0, 0). The lines are phase boundaries for the ground state of the system. The circles show the phase boundaries at $T = 500$ K. The numbers *1* and *2* indicate the fields of the ordered phases $C(2 \times 2)_A$ and $C(2 \times 2)_B$, respectively.

anism. It will be shown below that critical phenomena can occur at lower, more realistic, absolute values of the lateral interaction energy. For the above energy values, the following phases can exist in the adsorption layer: lattice gas (LG); lattice liquid of species A (LL_A); lattice liquid of species B (LL_B); checkerboard-type ordered phases of species A, B, and A + B ($C(2 \times 2)_A$, $C(2 \times 2)_B$, and $(C(2 \times 2)_{AB})$. The structures of these phases at $T = 0$ (T is absolute temperature in kelvins) are shown in Fig. 2. For each of the phases, one can readily write an expression for the thermodynamic potential Ω per cell at $T = 0$:

$$\text{LG: } \Omega = 0;\ \text{LL}_A\text{: } \Omega = 2\varepsilon_{AA} - \mu_A;\ \text{LL}_B\text{: } \Omega = 2\varepsilon_{BB} - \mu_B;$$
$$C(2 \times 2)_A\text{: } \Omega = -\mu_A/2;\ C(2 \times 2)_B\text{: } \Omega = -\mu_B/2; \quad (4)$$
$$C(2 \times 2)_{AB}\text{: } \Omega = 2\varepsilon_{AB} - (\mu_A + \mu_B)/2.$$

From Eq. (4), it is possible to derive the phase diagram of the ground state ($T = 0$) of the system for any set of nearest neighbor lateral interaction energies on the (μ_A, μ_B) plane. By way of example, we present the phase diagrams for the lateral interaction energy sets (10, –10, –10) and (10, 0, 0) on this plane (Fig. 3). Hereafter, in the interaction energy sets (a, b, c) $\varepsilon_{AA} = a$, $\varepsilon_{AB} = b$, and $\varepsilon_{BB} = c$ (kJ/mol). Obviously, the phase diagrams at nonzero temperatures will be different. However, at moderate temperatures, they will retain the structure shown in Fig. 3, except for the degenerate case of the absence of lateral interactions. All further calculations were carried out for $T = 500$ K, a temperature not very high for the preset absolute values of the lateral interaction energy. Therefore, the $T = 500$ K diagrams are qualitatively similar to the ground-state diagrams of the adsorption layer.

In order to substantiate this statement, we numerically constructed the $T = 500$ K phase diagram for the adsorption layer with the interaction energy set (10, –10, –10). The diagram was constructed by the Monte-Carlo method applied to a grand canonical ensemble. This was done using a technique based on the examination of susceptibilities and fourth-order Binder's cumulants of order parameters [30]. Following a procedure reported by Rzysko et al. [31], we divided the lattice into four equivalent sublattices and changed to spin variables according to the following rule: if the cell is occupied by a type A species, then $S = 1$; if the cell is occupied by a type B species, then $S = -1$; if the cell is vacant, then $S = 0$. The average magnetization of each sublattice was determined using the formula

$$m_k = \frac{1}{L^2}\sum_{i \in k} S_i, \quad (5)$$

where k is the index of one of the four equivalent sublattices and L is the lattice size. Combining the average magnetizations of the sublattices in various ways for each possible phase, one can make up a convenient order parameter. For example, the order parameter

$$\Psi = m_1 + m_2 + m_3 + m_4 \quad (6)$$

is equal to 0.5 for the $C(2 \times 2)_A$ and $C(2 \times 2)_B$ phases. We considered four different order parameters. For each of them, we related the corresponding susceptibility

$$\chi_\Psi = \frac{1}{RT}[\langle \Psi^2 \rangle - \langle |\Psi| \rangle^2] \quad (7)$$

and the fourth-order cumulant

$$U_\Psi = 1 - \frac{\langle \Psi^4 \rangle}{3\langle \Psi^2 \rangle^2} \quad (8)$$

to the chemical potential.

Note that, from the standpoint of the classification of phases according to their symmetry, there is no significant difference between the $C(2 \times 2)_A$, $C(2 \times 2)_B$, and $C(2 \times 2)_{AB}$ phases and the transitions between these

phases must be first-order. The transitions between these phase and the disordered phases LG, LL_A, and LL_B will obviously be second-order. Our numerical analysis has confirmed these inferences.

Exploration of the phase diagrams was beyond the scope of this study, so we limited ourselves to $L = 24$, 32, and 48 in our numerical calculations. For each chemical potential value, we made 2×10^5 Monte-Carlo steps, with averaging in the last 1.5×10^5 steps at 10-step intervals. The accuracy of this procedure was quite adequate to our analysis [30, 31]. The phase diagram thus constructed is very similar to the diagram of the adsorption layer in the ground state presented in Fig. 3a. The phase transition points numerically calculated for $T = 500$ K are also mapped here. The only difference between the ground-state and $T = 500$ K diagrams is that the fields of the checkerboard-type phases in the latter are slightly narrower.

In the framework of the lattice gas model and transition state theory, under the assumption that the adsorption layer is thermodynamically equilibrated, it is possible to obtain exact expressions for the rates of elementary processes, such as adsorption, desorption, and chemical reactions [32]. We will assume that the activated complexes in these processes do not interact with their environment. Introducing the designations $u = 2k_1 P_{A_2}/k_3$, $v = k_2 P_B/k_3$, $w = 2k_{-1}/k_3$, $s = k_{-2}/k_3$, $\overline{\mu_A} = \mu_A/RT$, $\overline{\mu_B} = \mu_B/RT$, and $\tau = k_3 t$ for the LH reaction, we arrive at the following set of kinetic equations:

$$\begin{cases} d\theta_A/d\tau = p_{00}(u - w\exp(2\overline{\mu_A}) - \exp(\overline{\mu_A} + \overline{\mu_B})) \\ d\theta_B/d\tau = v(1 - \theta_A - \theta_B) \\ - s(1 - \theta_A - \theta_B)\exp(\overline{\mu_B}) - p_{00}\exp(\overline{\mu_A} + \overline{\mu_B}), \end{cases} \quad (9)$$

where p_{00} is the probability of two adjacent sites being vacant and R is the universal gas constant.

The set of differential equations (9) in general form cannot be solved analytically, because the functions $p_{00}(\overline{\mu_A}, \overline{\mu_B})$, $\theta_A(\overline{\mu_A}, \overline{\mu_B})$, and $\theta_B(\overline{\mu_A}, \overline{\mu_B})$ cannot be represented in analytical form for the two-dimensional LG model. As was demonstrated earlier, one of the most efficient approximate methods for calculating these functions is the transfer matrix method [33–35]. The elements of the transfer matrix for the adsorption layer model considered were presented in our earlier publication [34].

The main advantage of the transfer matrix method is that the grand statistical sum is determined by its eigenvalue that is the largest in absolute magnitude and that the probabilities of various configurations can be derived from the corresponding eigenvector [34, 36]. Thus, the transfer matrix method provides a means to calculate the functions $p_{00}(\overline{\mu_A}, \overline{\mu_B})$, $\theta_A(\overline{\mu_A}, \overline{\mu_B})$, and $\theta_B(\overline{\mu_A}, \overline{\mu_B})$ that appear in the set of equations (9). The relevant computational algorithms are detailed elsewhere [34, 37–40].

In order to solve the set of differential equations (9), it is necessary to relate the chemical potentials μ_A and μ_B to the coverages (surface concentrations) θ_A and θ_B. As mentioned above, the transfer matrix method provides inverse relationships. Therefore, it is appropriate to change from the variables (θ_A, τ) and (θ_B, τ) to the variables $(\overline{\mu_A}, \tau)$ and $(\overline{\mu_B}, \tau)$. This change of variables is allowable if the corresponding Jacobian is nondegenerate. It can be demonstrated that the Jacobian is always nondegenerate for the LG model on the semi-infinite lattice considered in the transfer matrix method. The set of equations (9) in the new variables appears as

$$\begin{cases} \dfrac{d\overline{\mu_A}}{d\tau} = \dfrac{1}{\Delta}\dfrac{\partial\theta_B}{\partial\overline{\mu_B}}(u - w\exp(2\overline{\mu_A}) - \exp(\overline{\mu_A} + \overline{\mu_B}))p_{00} \\ - \dfrac{1}{\Delta}\dfrac{\partial\theta_A}{\partial\overline{\mu_B}}((v - s\exp(\overline{\mu_B}))(1 - \theta_A - \theta_B) \\ - p_{00}\exp(\overline{\mu_A} + \overline{\mu_B})) \\ \dfrac{d\overline{\mu_B}}{d\tau} = -\dfrac{1}{\Delta}\dfrac{\partial\theta_B}{\partial\overline{\mu_A}}(u - w\exp(2\overline{\mu_A}) - \exp(\overline{\mu_A} + \overline{\mu_B}))p_{00} \\ + \dfrac{1}{\Delta}\dfrac{\partial\theta_A}{\partial\overline{\mu_A}}((v - s\exp(\overline{\mu_B}))(1 - \theta_A - \theta_B) \\ - p_{00}\exp(\overline{\mu_A} + \overline{\mu_B})), \end{cases} \quad (10)$$

where Δ is the Jacobian of the change from the variables (θ_A, θ_B) to the variables $(\overline{\mu_A}, \overline{\mu_B})$.

Like the initial set of equations (9), the set of differential equations (10) is stiff for many values of adsorption layer model parameters and for many values of the rate constants of the LH mechanism steps. In the construction of phase portraits and kinetic curves for the set of equations (10), we used the Kaps–Rentrop algorithm, which implements the Rosenbrock method with automatic optimization of the step width [41, 42]. This algorithm allows the stiff set of differential equations (10) to be solved with a suitable degree of accuracy of 10^{-5} or better. Note that most of the computer time is spent on the calculation of the right-hand sides of the set of equations (10).

RESULTS AND DISCUSSION

For systematic analysis of the effect of the lateral interactions on the possibility of self-oscillations in the LH reaction with reversible and irreversible adsorption, we carried out a parametric analysis of the set of equations (10) for the nearest neighbor interaction energies ε_{AA}, ε_{AB}, and ε_{BB} equal to 10, –10, or 0 kJ/mol at 500 K. A total of 27 sets of energies were considered to include

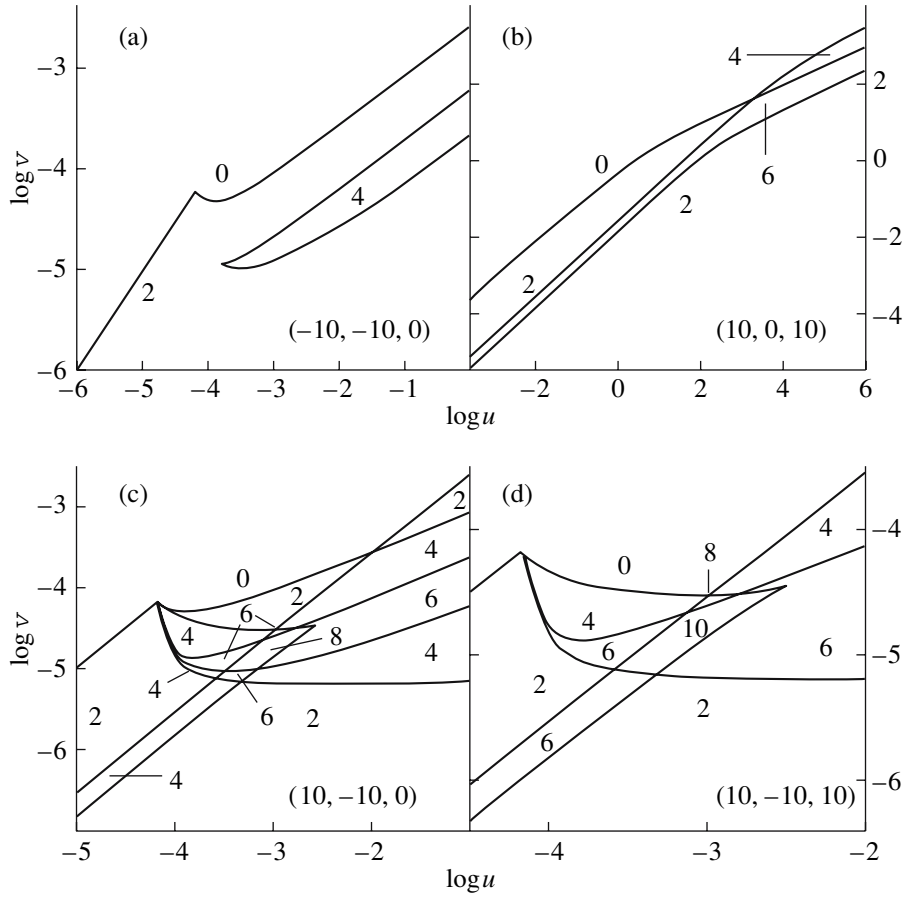

Fig. 4. Steady-state multiplicity diagram for irreversible adsorption, showing the numbers of interior steady states. The corresponding lateral interaction energy sets are given in parentheses.

all the possible signatures. In the calculation of the right-hand sides of the set of equations (10), we set $M = 4$, where M is the width of the infinite strip used in the transfer matrix method [34, 38, 39]. Sample calculations demonstrated that increasing the parameter M does not cause any qualitative changes and only slightly modifies the quantitative characteristics of the system.

For each of the 27 sets of lateral interaction energies, we constructed a steady state multiplicity diagram on the ($\log u$, $\log v$) plane for irreversible adsorption. A computational experiment demonstrated that the number of interior steady states is at least ten. A general analysis led us to conclude that a rather complicated set of lateral interaction energies can generate any number of interior steady states. Examples of constructed steady-state multiplicity diagrams are given in Fig. 4, which indicates the numbers of interior steady states, as well as the lateral interaction energies (kJ/mol) in parentheses. For the parameters specified above, the possible number of interior steady states ranges between 4 and 10. Note that, for all sets of lateral interaction energies for which the steady-state multiplicity diagram is topologically equivalent to the steady state multiplicity diagram for the ideal adsorption layer, the phase diagrams are also topologically equivalent. As mentioned above, the real lateral interaction energy is lower than 10 kJ/mol by a factor of 1.5–2. As the lateral interaction energy is decreased, the steady-state multiplicity diagram is simplified. However, even for the energy set (3.5, –3.5, 0) at $T = 500$ K, it has an area with four interior steady states.

The reversibility of the monomolecular adsorption step has a very strong effect on the steady state multiplicity diagram. As the reversibility parameter of this step (s) increases, the diagram is gradually simplified. It was demonstrated for the ideal adsorption layer [1] that there is no multiplicity area for sufficiently large s values. The same is likely to be true for the nonideal case, at least above the critical temperature. The reversibility of the bimolecular adsorption step (w) has a much weaker effect on the steady-state multiplicity diagram, but the general tendency to simplification is observed as well. The overall effect of the reversibility of all steps can be viewed as additive in the first approximation. The effect of reversibility on the steady-state multiplicity diagram is illustrated in Fig. 5 for the interaction energy set (–10, 10, 10).

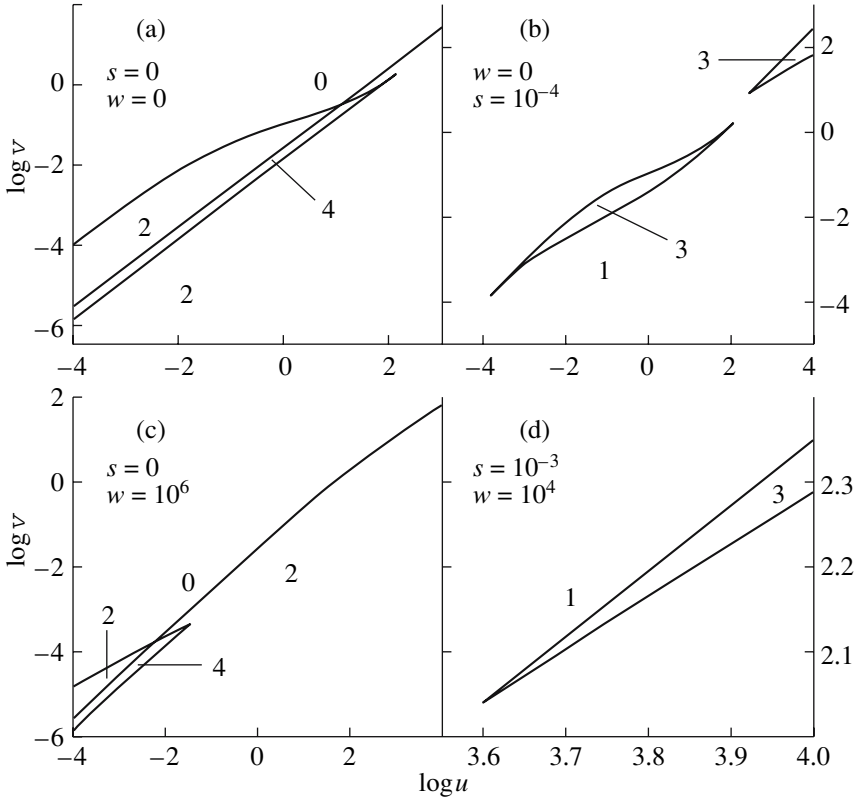

Fig. 5. Steady-state multiplicity diagram in the case of reversible adsorption for the lateral interaction energy set (–10, 10, 10). The numbers at the curves are the numbers of interior steady states.

A similar analysis was carried out for the simplest mechanism of monomolecular isomerization in a perfectly mixed reactor [43, 44]. It was demonstrated that any number of interior steady states can exist when there are lateral interactions in the adsorption layer.

Besides the steady-state multiplicity diagrams, bifurcation curves were mapped on the ($\log u$, $\log v$) plane. These curves separate an area in which the discriminant of the characteristic equation of the set of equations (10) is positive from an area where this discriminant is negative. Furthermore, we mapped the curves that are the locus of the points at which the sum of the roots of the characteristic equation is zero. In the linear approximation, the areas in which the discriminant of the characteristic equation is negative are the places in which stable or unstable focuses can exist. In the nonlinear approximation, these areas are the places where self-oscillations (i.e., limit cycles) can occur. A necessary condition for Andronov–Hopf bifurcation [45–47] is that the sum of the roots of the characteristic equation must be zero at a negative discriminant value.

Negative-discriminant areas on the parameter plane ($\log u$, $\log v$) were deduced for 9 of the 27 adsorption layer models examined. All these models are characterized by attraction between different types of species. Therefore, for the lateral interaction energy set considered, attraction between different species is the necessary and sufficient condition for the existence of an area where the discriminant of the characteristic equation is negative. For the nine models in the area with a negative discriminant, the phase portrait in the case of irreversible adsorption has focuses; for some of these models, the portrait has limit cycles. Limit cycles were deduced for seven of the nine lateral interaction energy sets. In all these cases, the limiting cycle results from Andronov–Hopf bifurcation. All of the discovered limit cycles are stable. Note that attraction between type B species prevents the existence of a limit cycle, except for the degenerate case (–10, –10, –10).

Self-oscillations in the models in which different types of species are attracted are likely due to the fact that the activation energy of the reaction between adsorbed species increases with increasing surface coverage, resulting in a nonmonotonic dependence of the reaction rate on the coverage.

Consider the effect of reversibility on the reaction rate self-oscillations. In general, the effect of reversibility on the existence of limit cycles is similar to its effect on the steady-state multiplicity area: the self-oscillations in the system are hampered as the reversibility parameter s increases. However, for two models in which different types of species are attracted, namely, (0, –10, –10) and (10, –10, –10), self-oscillations do not take place at $s = 0$ and appear at moderate s values. As s is further increased, they disappear again.

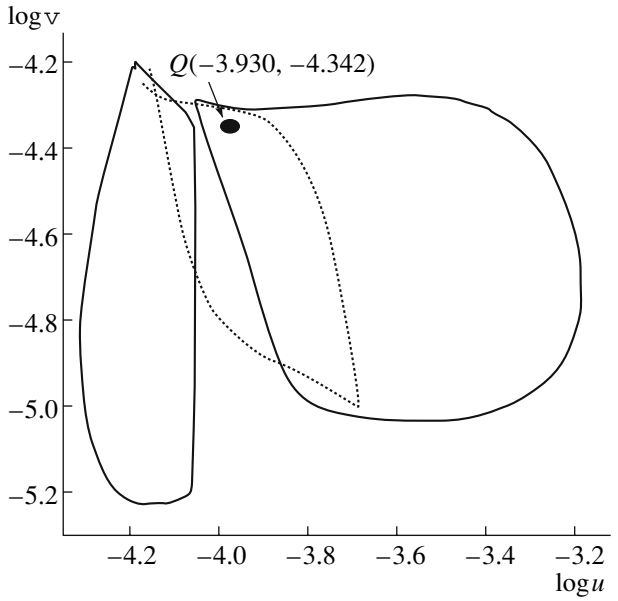

Fig. 6. Bifurcation diagram for the lateral interaction energy set (10, –10, 0) The phase portrait for the point Q(–3.930, –4.342) has a limit cycle.

In general, as follows from the ground-state phase diagrams of the of the adsorption layer models, self-oscillations are due to the existence of the ordered phase $C(2\times 2)_{AB}$. This phase exists in the last two models. The uncommon correlation between the occurrence of self-oscillations and the reversibility of the monomolecular adsorption step cannot be interpreted uniquely because of the complexity and the multiparametric character of the system. Note that, in some cases, as s grows, the steady state multiplicity region disappears earlier than the reaction rate oscillations. In particular, this interesting effect is observed for the (–10, –10, 0) and (–10, –10, 10) models at $s = 10^{-3}$. As in the case of the steady-state multiplicity diagrams, the reversibility of the bimolecular step on the self-oscillations is weaker than the effect of the monomolecular step.

For illustration, let us consider the results obtained for the (10, –10, 0) model, which allows eight interior steady states for irreversible adsorption. The steady-state multiplicity diagram for this model on the ($\log u$, $\log v$) plane is presented in Fig. 4c.

The solid line in Fig. 6 separates the regions with a negative and a positive discriminant of the characteristic equation, and the dashed line is the set of points at for which the sum of the roots of the characteristic equation is zero. The circle is the point Q(–3.930, –4.342), which lies in a region with two steady states. Intersecting the dashed line shown in Fig. 6 brings about Andronov–Hopf bifurcation and the appearance of a limit cycle in the system.

Figure 7 shows the phase portrait of the system in the (θ_A, θ_B) and (μ_A, μ_B) for the point Q(–3.930, –4.342).

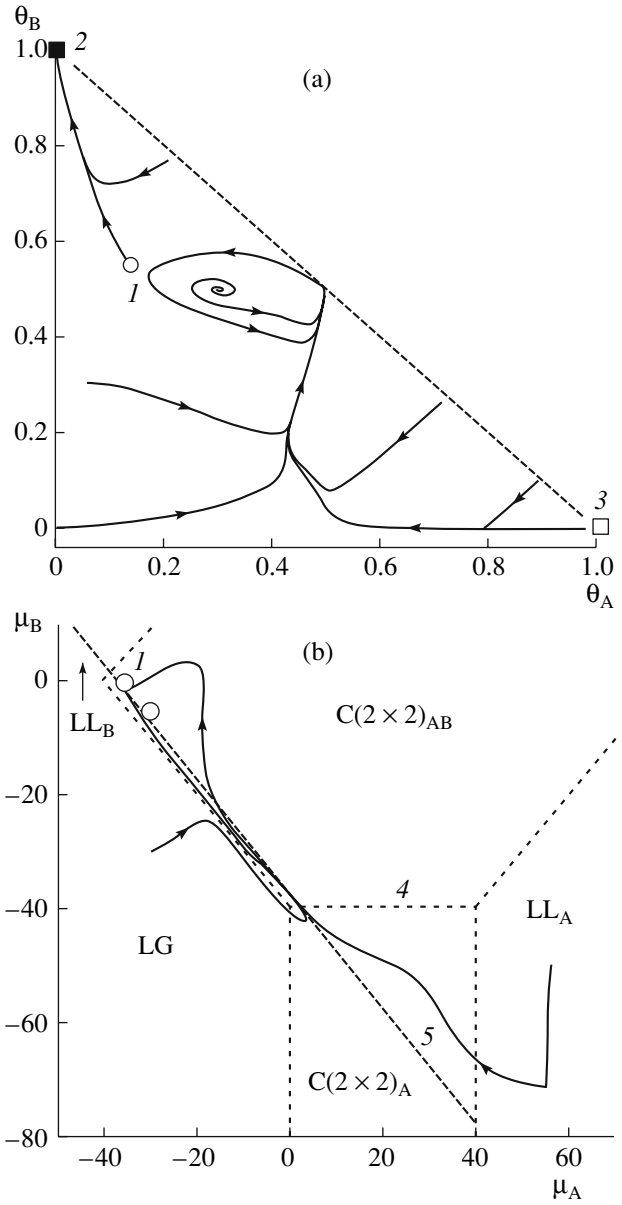

Fig. 7. Phase portrait for the point Q(–3.930, –4.342) on the (a) (θ_A, θ_B) and (b) (μ_A, μ_B) planes (see main text for explanation).

One can cleanly see the limit cycle due to the above-mentioned bifurcation. An unstable focus is inside the cycle. Circles *1* stand for unstable interior steady states, and squares *2* and *3* designate stable and unstable boundary steady states, respectively. Dashed lines *4* in Fig. 7b demarcate the fields of different surface phases. Interior steady-state points can lie only on dashed straight line *5*. The limit cycle lies almost entirely inside the field of the dense phase $C(2\times 2)_{AB}$. According to our calculations, this is a general situation. For the other models except the degenerate model (–10, –10, –10), the limit cycle also occurs inside this phase field.

The solid line in Fig. 8 shows the time dependence of the reaction rate for the phase trajectory originating

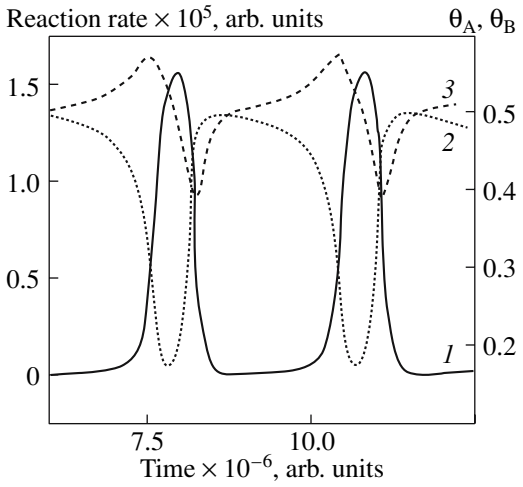

Fig. 8. (*1*) Reaction rate (in k_3 units), (*2*) compound A coverage, and (*3*) compound B coverage versus time (as $\tau = k_3 t$) for the trajectory portion corresponding to the limit cycle shown in Fig. 7.

from the unstable focus inside the limit cycle (see Fig. 7a). One can clearly see reaction rate self-oscillations. The amplitude of these self-oscillations is as high as two orders of magnitude. The dashed lines in Fig. 8 show the time dependences of the compound A (line *2*) and compound B (line *3*) coverages of the surface. The reaction rate in arbitrary units is plotted along the left-hand ordinate; the surface coverage, along the right-hand ordinate. The rate minimum, $\sim 10^{-7}$, corresponds to the state of the surface such that the A and B coverages are both 0.5, as in the ideal $C(2 \times 2)_{AB}$ structure. If the lateral interaction energy set is taken into account, the activation energy of desorption is the highest at this point. The reaction rate maximum approximately corresponds to the smallest value of the compound A coverage ($\theta_{A,\,min} \approx 0.17$). Note that the A coverage oscillation amplitude far exceeds the B coverage oscillation amplitude.

As the lateral interaction energies are decreased, the self-oscillation region diminishes and then vanishes. However, there are quite realistic lateral interaction energies, for example, (6, –6, 0) at which self-oscillations can take place.

CONCLUSIONS

Within the framework of the physically correct model of a nonideal adsorption layer, it has been demonstrated that the kinetic behavior of the LH mechanism is much more complicated for the nonideal layer than for the ideal layer. In the case of irreversible adsorption, there can be ten or even more interior steady states. General analysis suggests that a complicated set of lateral interaction energies can generate any number of interior steady states.

Reaction rate self-oscillations resulting from Andronov–Hopf bifurcation take place in some cases. Therefore, they can be described without introducing extra steps into the LH mechanism.

The complexity of the steady-state multiplicity diagram is intimately related to the complexity of the phase diagram of the adsorption layer. The self-oscillations of the reaction rate are due to the existence of the ordered phase $C(2 \times 2)_{AB}$.

REFERENCES

1. Bykov, V.I., Elokhin, V.I., Gorban, A.N., and Yablonski, G.S., *Comprehensive Chemical Kinetics*, vol. 32: *Kinetic Models of Catalytic Reactions*, Compton, R.G., Ed., Amsterdam: Elsevier, 1991.
2. Slinko, M.M. and Jaeger, N.I., *Oscillatory Heterogeneous Catalytic Systems*, Amsterdam: Elsevier, 1994.
3. Zhdanov, V.P., *Surf. Sci. Rep.*, 2002, vol. 45, p. 231.
4. Sales, B., Turner, J., and Maple, M., *Surf. Sci.*, 1982, vol. 114, p. 381.
5. Keren, I. and Sheintuch, M., *Chem. Eng. Sci.*, 2000, vol. 55, p. 1461.
6. Lanterbach, J., Bonilla, G., and Pleteher, T.D., *Chem. Eng. Sci.*, 1999, vol. 54, p. 4501.
7. Nekhamkina, O. and Sheintuch, M., *J. Chem. Phys.*, 2005, vol. 122, no. 19, p. 194701.
8. Digilov, R.M., Nekhamkina, O., and Sheintuch, M., *J. Chem. Phys.*, 2006, vol. 124, no. 3, p. 034709.
9. Luss, D. and Sheintuch, M., *Catal. Today*, 2005, vol. 105, p. 254.
10. Ziff, R.M., Gulari, E., and Barshad, Y., *Phys. Rev. Lett.*, 1986, vol. 56, p. 2553.
11. Evans, J.W., *J. Chem. Phys.*, 1993, vol. 98, no. 3, p. 2463.
12. Lutsevich, L.V., Elokhin, V.I., Myshlyavtsev, A.V., Usov, A.G., and Yablonskii, G.S., *J. Catal.*, 1991, vol. 132, p. 302.
13. Hua, D.-J., *Phys. Rev. E: Stat. Phys., Plasmas, Fluids, Relat. Interdiscip. Top.*, 2004, vol. 70, no. 6, p. 066101.
14. Machado, E., Buendia, G.M., and Rikvold, P.A., *Phys. Rev. E: Stat. Phys., Plasmas, Fluids, Relat. Interdiscip. Top.*, 2005, vol. 71, no. 3, p. 031 603.
15. Machado, E., Buendia, G.M., Rikvold, P.A., and Ziff, R.M., *Phys. Rev. E: Stat. Phys., Plasmas, Fluids, Relat. Interdiscip. Top.*, 2005, vol. 71, no. 1, p. 016120.
16. Laurin, N., Johanek, V., Grant, A.W., Kasemo, B., Libuda, J., and Freund, H.-J., *J. Chem. Phys.*, 2005, vol. 123, no. 5, p. 054701.
17. Wang, J., *J. Chem. Phys.*, 2003, vol. 119, p. 3626.
18. Cordoba, A., Lemos, M.C., and Jimenez-Morales, F., *J. Chem. Phys.*, 2006, vol. 124, no. 1, p. 014707.
19. Pavlenko, N., Imbihl, R., Evans, J.W., and Liu, D.-J., *Phys. Rev. E: Stat. Phys., Plasmas, Fluids, Relat. Interdiscip. Top.*, 2003, vol. 68, no. 1, p. 016212.
20. Evans, J.W., Liu, D.-J., and Tammaro, M., *Chaos*, 2002, vol. 12, p. 131.
21. Hou, Z., Rao, T., and Xin, H., *J. Chem. Phys.*, 2005, vol. 122, no. 3, p. 034708.

22. Pineda, M., Imbihl, R., Schimansky-Geier, L., and Zulicke, Ch., *J. Chem. Phys.*, 2006, vol. 124, no. 4, p. 044701.
23. Peskov, N.V., Slinko, M.M., Carabineiro, S.A.C., and Nieuwenhuys, B.E., *Papers from the Int. Conf. in Nonlinear Sciences*, Belgrade, 2004, p. 101.
24. Araya, P. and Cortes, J., *J. Chem. Phys.*, 1994, vol. 101, no. 2, p. 1668.
25. Gelten, R.J., Jansen, A.P.J., van Santen, R.A., Lukkien, J.J., Segers, J.P.L., and Hilbers, P.A.J., *J. Chem. Phys.*, 1998, vol. 108, p. 5921.
26. Zhdanov, V.P. and Kasemo, B., *J. Chem. Phys.*, 2001, vol. 114, p. 5351.
27. Gerrard, A.L. and Weaver, J.F., *J. Chem. Phys.*, 2005, vol. 123, no. 22, p. 224703.
28. Boreskov, G.K., *Geterogennyi kataliz* (Heterogeneous Catalysis), Moscow: Nauka, 1986.
29. Gorban', A.N., Bykov, V.I., and Yablonskii, G.S., *Ocherki o khimicheskoi relaksatsii* (Topics in Chemical Relaxation), Novosibirsk: Nauka, 1986.
30. Landau, D.P. and Binder, K.A., *Guide to Monte Carlo Simulation in Statistical Physics*, Cambridge: Cambridge Univ. Press, 2000, p. 383.
31. Rzysko, W., Patrykiejew, A., and Binder, K., *Phys. Rev. B: Condens. Matter*, 2005, vol. 72, no. 16, p. 165416.
32. Zhdanov, V.P., *Elementarnye fiziko-khimicheskie protcessy na poverkhnosti* (Elementary Physicochemical Surface Processes), Novosibirsk: Nauka, 1988.
33. Myshlyavtsev, A.V. and Zhdanov, V.P., *Chem. Phys. Lett.*, 1989, vol. 162, no. 1, p. 43.
34. Myshlyavtsev, A.V. and Myshlyavtseva, M.D., *Vychislitel'nye aspekty metoda transfer-matritsy* (Computational Aspects of the Transfer Matrix Method), Kyzyl: TuvIKOPR, 2000, p. 101.
35. Bykov, V.I., Myshlyavtsev, A.V., and Slin'ko, M.G., *Dokl. Akad. Nauk*, 2002, vol. 384, no. 5, p. 650 [*Dokl. Chem.* (Engl. Transl.), vol. 384, no. 5, p. 170].
36. Baxter, R.J., *Exactly Solved Models in Statistical Mechanics*, London: Academic, 1982, p. 486.
37. Myshlyavtsev, A.V. and Dongak, M.D., *J. Stat. Phys.*, 1997, vol. 87, p. 593.
38. Runnels, L.K. and Combs, L.L., *J. Chem. Phys.*, 1966, vol. 45, p. 2482.
39. Bartlet, N.C., Einstein, T.L., and Roelofs, L.D., *Phys. Rev. B: Condens. Matter*, 1986, vol. 34, p. 1616.
40. Myshlyavtsev, A.V., Sales, J.L., Zgrablich, G., and Zhdanov, V.P., *J. Stat. Phys.*, 1990, vol. 58, p. 1029.
41. Shampine, L.F. and Gordon, M.K., *Computer Solution of Ordinary Differential Equations: The Initial Value Problem*, San-Francisco: Freeman, 1975.
42. Press, W.H., Teukolsky, S.A., Vetterling, W.T., and Flannery, B.P., *Numerical Recipes in Fortran 77: The Art of Scientific Computing*, Cambridge: Cambridge Univ. Press, 1992, vol. 1.
43. Myshlyavtsev, A.V., Samdanchap, R.T., and Yablonskii, G.S., *Kinet. Katal.*, 1992, vol. 33, nos. 5–6, p. 1220.
44. Myshlyavtsev, A.V., Yablonskii, G.S., and Samdanchap, R.T., *React. Kinet. Catal. Lett.*, 1994, vol. 53, p. 269.
45. Andronov, A.A. and Pontryagin, L.S., *Dokl. Akad. Nauk SSSR*, 1937, vol. 14, p. 247.
46. Arrowsmith, D.K. and Place, C.M., *Ordinary Differential Equations: A Qualitative Approach with Applications*, London: Chapman & Hall, 1982, p. 243.
47. Crawford, J.D., *Rev. Mod. Phys.*, 1991, vol. 63, no. 4, p. 991.